RECONSTRUCTION OF INCLUSIONS IN AN ELASTIC BODY

GUNTHER UHLMANN, JENN-NAN WANG, AND CHIN-TIEN WU

ABSTRACT. We consider the reconstruction of elastic inclusions embedded inside of a planar region, bounded or unbounded, with isotropic inhomogeneous elastic parameters by measuring displacements and tractions at the boundary. We probe the medium with complex geometrical optics solutions having polynomial-type phase functions. Using these solutions we develop an algorithm to reconstruct the exact shape of a large class of inclusions including star-shaped domains and we implement numerically this algorithm for some examples.

1. INTRODUCTION

The purpose of this paper is several fold. First, we provide numerical evidence for the algorithms developed in [12] and [13] for determining elastic inclusions embedded in an inhomogeneous background. Second we extend, and simplify, the object identification result in [9] from the conductivity equation on an infinite slab to the elasticity system. Third we also develop a numerical algorithm for the case of the infinite slab and we test it numerically. Our main method is to use complex geometrical optics (CGO) solutions with general phases constructed in [13] to treat the inverse problems.

We consider the problems in the plane. Let Ω be an open domain in $\mathbb{R}^2$ with smooth boundary $\partial\Omega$ which is not necessarily bounded. The domain Ω is filled with an inhomogeneous, isotropic, elastic medium characterized by the Lamé parameters $\lambda(x)$ and $\mu(x)$. Assume that $\lambda(x) \in C^2(\overline{\Omega})$, $\mu(x) \in C^4(\overline{\Omega})$ and the following inequalities hold

$$\mu(x) > 0 \quad \text{and} \quad \lambda(x) + 2\mu(x) > 0 \quad \forall\, x \in \overline{\Omega} \quad \text{(strong ellipticity)}. \tag{1.1}$$

We consider the static isotropic elasticity system without sources

$$\mathcal{L}u := \nabla \cdot (\lambda(\nabla \cdot u)I + 2\mu S(\nabla u)) = 0 \quad \text{in} \quad \Omega. \qquad (1.2)$$

Here and below, $S(A) = (A + A^T)/2$ denotes the symmetric part of the matrix $A \in \mathbb{C}^{2\times 2}$. Equivalently, if we denote $\sigma(u) = \lambda(\nabla \cdot u)I + 2\mu S(\nabla u)$ the stress tensor, then (1.2) becomes

$$\nabla \cdot \sigma = 0 \quad \text{in} \quad \Omega.$$

On the other hand, since the Lamé parameters are differentiable, we can also write (1.2) in the non-divergence form

$$\mu \Delta u + (\lambda + \mu)\nabla(\nabla \cdot u) + \nabla\lambda\nabla \cdot u + 2S(\nabla u)\nabla\mu = 0 \text{ in } \Omega. \qquad (1.3)$$

Recently, a framework of constructing CGO solutions with general phases for systems with the Laplacian as the leading part was proposed by the first two authors [13]. The elasticity system (1.2) is among the systems considered in [13]. To simplify the presentation, we will not go over the development of CGO solutions and their important role in inverse problems. For more details, we refer to [10, 11] and references therein.

To really appreciate the usefulness of CGO solutions with general phases, we shall study the inverse problem with an unbounded background domain. Ikehata in [5] considered the inverse conductivity problem in an infinite slab where the location of an inclusion is reconstructed by infinitely many boundary measurements. In [5], he used Calderón type harmonic functions [1], i.e., $e^{x\cdot(\omega+i\omega^\perp)}$ with $\omega \in \mathbb{S}^{n-1}$. These functions are not integrable on hyperplanes. To remedy this, he introduced Yarmukhamedov's Green function to construct a sequence of harmonic functions with finite energy that approximate the Calderón type function on a bounded part of the slab and are arbitrarily small on an unbounded part of the slab.

In [9] the authors used complex spherical waves rather than Calderón type functions for the object identification problem in the slab. The most obvious advantage is that they do not need Yarmukhamedov's Green function to "localize" complex spherical waves since these solutions decay faster than any given polynomial order on infinite hyperplanes. In this work, we extend the result in [9] to the elasticity system (1.2). We also simplify some arguments in [9]. Likewise, we consider the object identification problem in an infinite strip. As in [13], we will use CGO solutions with phases being complex polynomials. For these solutions, the probing fronts are confined in a suitable cone. By increasing the degree of the polynomial, one can shrink the opening

angle of the cone and, therefore, squeeze the probing fronts. We re-mark that the probing fronts of complex spherical waves are spheres or circles. In other words, we are able to determine more information of the unknown object using CGO solutions with polynomial phases.

For the reconstruction of the unknown object in two dimensions, we would like to mention an interesting result by Ikehata in [6] where he introduced the Mittag-Leffler function in his method. The numerical implementation of [6] was carried out by Ikehata and Siltanen in [7]. However, the approach with the Mittag-Leffler function can not be applied to the isotropic elasticity system even when the medium is homogeneous.

This paper is organized as follows. In Section 2, we show how to construct CGO solutions with general phases for the elasticity system. In Section 3, we apply these CGO solutions to study the reconstruction of inclusions by boundary measurements and give a numerically feasible algorithm. In Section 4, we provide some computational results with simulated data.

2. CGO SOLUTIONS WITH GENERAL PHASES FOR THE ELASTICITY SYSTEM

In this section we recall the construction of CGO solutions to (1.2) outlined in [13]. To do so, we first reduce the system to the one with the Laplacian as the leading part. We will use the reduced system derived by Ikehata (see for instance [4], [10]). Let $\begin{pmatrix} w \\ g \end{pmatrix}$ satisfy

$$\Delta \begin{pmatrix} w \\ g \end{pmatrix} + A(x) \begin{pmatrix} \nabla g \\ \nabla \cdot w \end{pmatrix} + Q(x) \begin{pmatrix} w \\ g \end{pmatrix} = 0, \qquad (2.1)$$

where

$$A(x) = \begin{pmatrix} 2\mu^{-1/2}(-\nabla^2 + \Delta)\mu^{-1} & -\nabla \log \mu \\ 0 & \frac{\lambda+\mu}{\lambda+2\mu}\mu^{1/2} \end{pmatrix}$$

and

$$Q(x) = \begin{pmatrix} -\mu^{-1/2}(2\nabla^2 + \Delta)\mu^{1/2} & 2\mu^{-5/2}(\nabla^2 - \Delta)\mu \, \nabla\mu \\ -\frac{\lambda-\mu}{\lambda+2\mu}(\nabla\mu^{1/2})^T & -\mu\Delta\mu^{-1} \end{pmatrix}.$$

Here $\nabla^2 f$ is the Hessian of the scalar function f. Then

$$u := \mu^{-1/2}w + \mu^{-1}\nabla g - g\nabla\mu^{-1} \qquad (2.2)$$

satisfies (1.3).

Now let Ω_0 be a suitable subdomain of Ω and $\rho(x) = \varphi(x) + i\psi(x)$ be conformal in Ω_0. Moreover, we assume that $\rho(x)$ is a diffeomorphism

in Ω_0. Then we can find $U(x)$ satisfying (2.1) in Ω_0 with

$$U(x) = \begin{pmatrix} w \\ g \end{pmatrix} = e^{(\varphi + i\phi)/h}(L + R) \tag{2.3}$$

for some three-dimensional vectors L and R, where L is independent of h and R satisfies

$$\|\partial^\alpha R\|_{L^2(\Omega_0)} \le Ch^{1-\alpha}, \quad \forall \, |\alpha| \le 2. \tag{2.4}$$

Our method of constructing $U(x)$ in the form (2.3) goes as follows. Let (y_1, y_2) be the new coordinates defined by $y_1 = \varphi(x)$ and $y_2 = \psi(x)$. In the new coordinates (y_1, y_2), (2.1) is transformed into

$$\Delta \begin{pmatrix} \tilde{w} \\ \tilde{g} \end{pmatrix} + \tilde{A}(y, D) \begin{pmatrix} \tilde{w} \\ \tilde{g} \end{pmatrix} + \tilde{Q}(y) \begin{pmatrix} \tilde{w} \\ \tilde{g} \end{pmatrix} = 0, \tag{2.5}$$

where $\tilde{A}(y, D)$ is a first order differential operator. Using the Carleman technique or the method of intertwining operators [8], one can construct CGO solutions to (2.5) with linear phases, namely,

$$\tilde{U}(y) = \begin{pmatrix} \tilde{w} \\ \tilde{g} \end{pmatrix} = e^{(y_1 + iy_2)/h}(\tilde{L} + \tilde{R}).$$

Then to get (2.3), we simply make a change of coordinates $y \to x$, i.e. $U(x) = \tilde{U}(y(x))$ (see [13] for more details). The key idea in this approach is that the Laplacian is invariant under conformal mappings. Hence, if we take u as the form (2.2), then u is a CGO solution to (1.2) in Ω_0. We want to remark that L is a non-zero vector satisfying a Cauchy-Riemann type equation. Denote $L = \begin{pmatrix} \ell \\ d \end{pmatrix}$ with $\ell \in \mathbb{C}^2$ and $d \in \mathbb{C}^1$. Generically, we can assume that both ℓ and d do not vanish in Ω_0 (see [12, Remark 3.1 and 4.1]).

Due to the conformality of ρ, φ and ψ are harmonic functions in Ω_0. Conversely, given any φ harmonic in Ω_0 with $\nabla\varphi \ne 0$ in Ω_0, we can find a harmonic conjugate ψ of φ in Ω_0 so that $\rho = \varphi + i\psi$ is conformal in Ω_0. The freedom of choosing φ plays a key role in our reconstruction method for the object identification problem. Actually, we will mainly focus on level curves of φ. As in [13], we choose $\rho(x)$ to be complex polynomials.

Pick a point $x_0 \notin \bar{\Omega}$. It is no restriction to assume $x_0 = 0$. We now consider $\varphi_N = \text{Re}(c_N x^N)$ for $N \ge 2$, where $c_N \in \mathbb{C}$ with $|c_N| = 1$. In the polar coordinates, $\varphi_N(r, \theta) = r^N \cos N(\theta - \theta_N)$ for some θ_N determined by c_N. We observe that $\varphi_N > 0$ in some open cone Γ_N with an opening angle π/N. Now assume that $\Gamma_N \cap \Omega \ne \emptyset$. The complex function $\rho_N(x) = c_N x^N = \varphi_N + i\psi_N$ is clearly conformal in Ω. For

solving the inverse problem, we want to shrink the opening angle of Γ_N by taking $N \to \infty$. However, there are two serious problems in doing so. On one hand, φ_N is periodic in the angular variable, which means that it is positive in some other cones with the same opening angle which also intersect Ω when N is large. This property of φ_N prohibits us from using corresponding CGO solutions with large N to the object identification problem. On the other hand, the complex function $\rho_N(x)$ fails to be injective in the whole domain Ω when N is large. To overcome those difficulties and construct useful CGO solutions in the whole domain Ω, we shall carry out the construction described above in

$$\Omega_0 = \Gamma_N \cap \Omega$$

and extend the constructed solutions to Ω by cut-off functions. From now on, we assume that Ω_0 is bounded.

We first note that ρ_N is conformal in Ω_0 and is bijective from Ω_0 onto $\rho_N(\Omega_0)$. We denote

$$U_{N,h}(x) = \begin{pmatrix} w_{N,h} \\ g_{N,h} \end{pmatrix} = e^{(\varphi_N + i\psi_N)/h}(L + R)$$

solving (2.1) in Ω_0. That is,

$$u_{N,h} = \mu^{-1/2}w_{N,h} + \mu^{-1}\nabla g_{N,h} - g_{N,h}\nabla\mu^{-1}$$

satisfies (1.2) in Ω_0. Now to get solutions of (1.2) in the whole domain Ω, we use a cut-off technique. For $s > 0$, let $l_s = \{x \in \Gamma_N : \varphi_N = s^{-1}\}$. This is the level curve of ϕ_N in Γ_N. Let $0 < t < t_0$ such that

$$(\cup_{s \in (0,t)}l_s) \cap \Omega \neq \emptyset$$

and choose a small $\varepsilon > 0$. Define a cut-off function $\phi_{N,t}(x) \in C^\infty(\mathbb{R}^2)$ so that $\phi_{N,t}(x) = 1$ for $x \in \overline{(\cup_{s \in (0,t+\varepsilon/2)}l_s) \cap \Omega}$ and is zero for $x \in \bar{\Omega} \setminus (\cup_{s \in (0,t+\varepsilon)}l_s)$. We now define

$$u_{N,t,h}(x) = \phi_{N,t}e^{-t^{-1}/h}u_{N,h}$$

for $x \in (\cup_{s \in (0,t+\varepsilon)}l_s) \cap \Omega$. So $u_{N,t,h}$ can be regarded as a function in Ω which is zero outside of Ω_0. We now take $f_{N,t,h} = u_{N,t,h}|_{\partial\Omega}$. We remark that $f_{N,t,h}$ can be used as the boundary data in the inverse problem. An obvious reason of using $f_{N,t,h}$ is that they are local and so we only need to collect Neumann data over the support of $f_{N,t,h}$ when we study the object identification problem with boundary measurements. Note that since Ω_0 is bounded, we can see that $u_{N,t,h} \in H^1(\Omega)$ and therefore

$$f_{N,t,h} \in H^{1/2}(\partial\Omega).$$

The function $u_{N,t,h}$ is not a solution to the elasticity equation in Ω. However, we shall show that the difference between $u_{N,t,h}$ and the true solution to the elasticity equation with the same Dirichlet condition as $u_{N,t,h}$ is exponentially small. Precisely, let us consider the boundary value problem:

$$\begin{cases} \mathcal{L}w_{N,t,h} = 0 & \text{in} \quad \Omega \\ w_{N,t,h} = f_{N,t,h} & \text{on} \quad \partial\Omega. \end{cases} \tag{2.6}$$

Then we can show that

Lemma 2.1. *There exists a unique solution $w_{N,t,h}$ to (2.6). Moreover, there exist $C > 0$ and $\varepsilon' > 0$ such that*

$$\|u_{N,t,h} - w_{N,t,h}\|_{H^1(\Omega)} \leq C e^{-\varepsilon'/h} \tag{2.7}$$

Proof. Denote $\tilde{u}_{N,t,h} = u_{N,t,h} - w_{N,t,h}$. Then $\tilde{u}_{N,t,h}$ satisfies

$$\begin{cases} \mathcal{L}\tilde{u}_{N,t,h} = g_{N,t,h} & \text{in} \quad \Omega, \\ \tilde{u}_{N,t,h} = 0 & \text{on} \quad \partial\Omega, \end{cases}$$

where $g_{N,t,h} = \mathcal{L}u_{N,t,h}$. Note that $\mathcal{L}u_{N,h} = 0$ in $(\cup_{s\in(0,t_0)}l_s) \cap \Omega$ and $\partial_{x_j}\phi_{N,t}(x)$ for $j = 1, 2$ are supported in

$$\overline{(\cup_{s\in(t+\varepsilon/2,t+\varepsilon)}l_s) \cap \Omega}.$$

So $g_{N,t,h}$ is supported in $\overline{(\cup_{s\in(t+\varepsilon/2,t+\varepsilon)}l_s) \cap \Omega}$ and we have that

$$\|g_{N,t,h}\|_{L^2(\Omega)} \leq C' e^{-\varepsilon'/h} \tag{2.8}$$

for some $C' > 0$ and $\varepsilon' > 0$. Now the lemma follows from the first Korn inequality and the Lax-Milgram theorem. $\square$

3. Reconstruction of inclusions

We will use the special solutions constructed in the previous section to study the inverse problem of reconstructing embedded inclusions. Here we follow the presentation given in [12]. Assume that Ω is either a bounded domain or an infinite strip. Also, let $0 \notin \bar{\Omega}$ and $\Omega = \{(x_1, x_2) : x_1 \in \mathbb{R},\ a < x_2 < b < 0\}$ if Ω is a strip. Now consider D an open subset of Ω with Lipschitz boundary satisfying that $D \subset\subset \Omega$ and $\Omega \setminus \overline{D}$ is connected. Suppose that $\lambda_0(x) \in C^2(\overline{\Omega})$ and $\mu_0(x) \in C^4(\overline{\Omega})$ satisfy the strong convexity condition, i.e.,

$$3\lambda_0(x) + 2\mu_0(x) > 0 \quad \text{and} \quad \mu_0(x) > 0 \quad \forall \ x \in \overline{\Omega}. \tag{3.1}$$

It is obvious that (3.1) implies (1.1). On the other hand, we assume that $\widetilde{\lambda}(x), \widetilde{\mu}(x)$ be two essentially bounded functions such that either

$$\widetilde{\mu} \geq 0 \quad \text{and} \quad 3\widetilde{\lambda} + 2\widetilde{\mu} \geq 0 \quad \text{a.e. in} \quad D$$

or

$$\widetilde{\mu} \leq 0 \quad \text{and} \quad 3\widetilde{\lambda} + 2\widetilde{\mu} \leq 0 \quad \text{a.e. in} \quad D.$$

Furthermore, suppose that $\lambda = \lambda_0 + \chi_D \widetilde{\lambda}$ and $\mu = \mu_0 + \chi_D \widetilde{\mu}$ satisfy (3.1) a.e. in Ω, where χ_D is the characteristic function of D. Therefore, for any $f \in H^{1/2}(\partial\Omega)$, there exists a unique (weak) solution u to

$$\begin{cases} \mathcal{L}_D u = 0 & \text{in} \quad \Omega \\ u = f & \text{on} \quad \partial\Omega. \end{cases} \tag{3.2}$$

Here the elastic operator $\mathcal{L}_D$ is defined in terms of λ and μ. As before, we can prove the well-posedness of (3.2) by combining the first Korn inequality and the Lax-Milgram theorem. The arguments remain valid even when Ω is an infinite strip. The Dirichlet-to-Neumann map related to $\mathcal{L}_D$ is now defined as

$$\Lambda_D : f \rightarrow \sigma(u)\mathbf{n}|_{\partial\Omega}$$

where $\mathbf{n}$ is the unit outer normal of $\partial\Omega$ and for $x \in \partial\Omega$

$$\sigma(u) = \lambda(\nabla \cdot u)I + 2\mu S(\nabla u) = \lambda_0(\nabla \cdot u)I + 2\mu_0 S(\nabla u).$$

Now assume that all parameters are known except $\widetilde{\lambda}$, $\widetilde{\mu}$, and D. The inverse problem is to determine D by Λ_D. Here we will provide a reconstruction algorithm to this inverse problem. We begin with some useful integral inequalities. Let Λ_0 be the Dirichlet-to-Neumann map related to $\mathcal{L}_0$, where $\mathcal{L}_0$ is the elastic operator defined in terms of λ_0 and μ_0. Assume that u_0 is the solution of

$$\begin{cases} \mathcal{L}_0 u_0 = 0 & \text{in} \quad \Omega \\ u_0 = f & \text{on} \quad \partial\Omega. \end{cases} \tag{3.3}$$

Then one can derive the following inequalities

$$\int_D \{\frac{3\lambda_0 + 2\mu_0}{3(3\lambda + 2\mu)}(3\widetilde{\lambda} + 2\widetilde{\mu})|\nabla \cdot u_0|^2 + 2\frac{\mu_0}{\mu}\widetilde{\mu}|S(\nabla u_0) - \frac{\nabla \cdot u_0}{3}I|^2\}dx$$
$$\leq \quad \langle(\Lambda_D - \Lambda_0)f, \overline{f}\rangle$$
$$\leq \quad \int_D \frac{3\widetilde{\lambda} + 2\widetilde{\mu}}{3}|\nabla \cdot u_0|^2 + 2\widetilde{\mu}|S(\nabla u_0) - \frac{\nabla \cdot u_0}{3}I|^2\}dx \tag{3.4}$$

(see [3, Proposition 5.1]).

We are now at a position to discuss the inverse problem. First of all, we give an appropriate jump condition across ∂D:

for $y \in \partial D$, there exists a ball $B_\epsilon(y)$ such that *one* of the following conditions holds:

$$
\begin{cases}
\widetilde{\mu} > \epsilon, \ 3\widetilde{\lambda} + 2\widetilde{\mu} \geq 0 \\
\widetilde{\mu} = 0, \ \widetilde{\lambda} > \epsilon \\
\widetilde{\mu} < -\epsilon, \ 3\widetilde{\lambda} + 2\widetilde{\mu} \leq 0 \\
\widetilde{\mu} = 0, \ \widetilde{\lambda} < -\epsilon
\end{cases}
, \ \forall \ x \in B_\epsilon(y) \cap D.
\tag{3.5}
$$

Now let $w_{N,t,h}$ be the solution of (3.3) with the Dirichlet condition $f = f_{N,t,h}$. To construct the inclusion D, we rely on the quantity

$$
E(N,t,h) = \langle (\Lambda_D - \Lambda_0) f_{N,t,h}, \overline{f}_{N,t,h} \rangle.
$$

Clearly, this quantity is completely determined by the boundary data localized in $\Gamma_N \cap \partial\Omega$. This localization property is of great value in actual applications, especially when Ω is an infinite strip. Now $E(N,t,h)$ satisfies the integral inequality (3.4) with u_0 being replaced by $w_{N,t,h}$, i.e.

$$
\int_D \{ \frac{3\lambda_0 + 2\mu_0}{3(3\lambda + 2\mu)} (3\widetilde{\lambda} + 2\widetilde{\mu}) |\nabla \cdot w_{N,t,h}|^2 + 2\frac{\mu_0}{\mu}\widetilde{\mu} |S(\nabla w_{N,t,h}) - \frac{\nabla \cdot w_{N,t,h}}{3} I|^2 \} dx
$$
$$
\leq \ E(N,t,h)
$$
$$
\leq \ \int_D \frac{3\widetilde{\lambda} + 2\widetilde{\mu}}{3} |\nabla \cdot w_{N,t,h}|^2 + 2\widetilde{\mu} |S(\nabla w_{N,t,h}) - \frac{\nabla \cdot w_{N,t,h}}{3} I|^2 \} dx.
\tag{3.6}
$$

Argued as in [12] and [13], we can prove the following important behaviors of $E(N,t,h)$.

Theorem 3.1. *Let $t > 0$ and $\mathcal{D}_t = \{ x \in \Gamma_N : \varphi_N \geq t^{-1} \}$. Assume that one of the jump conditions (3.5) holds. Then we have:*
(i) if $\mathcal{D}_t \cap \bar{D} = \emptyset$ then there exist $C_1 > 0$, $\varepsilon_1 > 0$, and $h_1 > 0$ such that $E(N,t,h) \leq C_1 e^{-\varepsilon_1/h}$ for all $h \leq h_1$;
(ii) if $\mathcal{D}_t \cap D \neq \emptyset$ then there exist $C_2 > 0$, $\varepsilon_2 > 0$, and $h_2 > 0$ such that $E(N,t,h) \geq C_2 e^{\varepsilon_2/h}$ for all $h \leq h_2$.

Proof. The proof here relies on the integral inequalities (3.6). Replacing $w_{N,t,h}$ in (3.6) by $u_{N,t,h}$ and taking into account of (2.7) leads

to

$$\int_D \{\frac{3\lambda_0 + 2\mu_0}{3(3\lambda + 2\mu)}(3\widetilde{\lambda} + 2\widetilde{\mu})|\nabla \cdot u_{N,t,h}|^2 + 2\frac{\mu_0}{\mu}\widetilde{\mu}|S(\nabla u_{N,t,h}) - \frac{\nabla \cdot u_{N,t,h}}{3}I|^2\}dx$$
$$+O(e^{-\varepsilon'/h})$$
$$\leq \quad E(N,t,h)$$
$$\leq \quad \int_D \frac{3\widetilde{\lambda} + 2\widetilde{\mu}}{3}|\nabla \cdot u_{N,t,h}|^2 + 2\widetilde{\mu}|S(\nabla u_{N,t,h}) - \frac{\nabla \cdot u_{N,t,h}}{3}I|^2\}dx + O(e^{-\varepsilon'/h}) \quad (3.7)$$

Recall that

$$u_{N,t,h}(x) = \phi_{N,t}e^{-t^{-1}/h}u_{N,h}$$
$$= \phi_{N,t}e^{-t^{-1}/h}\{\mu_0^{-1/2}w_{N,h} + \mu_0^{-1}\nabla g_{N,h} - g_{N,h}\nabla\mu_0^{-1}\},$$

where $\begin{pmatrix} w_{N,h} \\ g_{N,h} \end{pmatrix}$ solves (2.1) in Ω with Lamé parameters λ_0 and μ_0. We now write

$$w_{N,h} = e^{(\varphi_N + i\psi_N)/h}(\ell + r) \quad \text{and} \quad g_{N,h} = e^{(\varphi_N + i\psi_N)/h}(d + s).$$

Through tedious but straightforward computations, the leading terms of $\nabla \cdot u_{N,t,h}$ and $S(\nabla u_{N,t,h})$ are respectively

$$e^{(\varphi_N - t^{-1} + i\psi_N)/h}\mu_0^{-1/2}(1 - \frac{\lambda_0 + \mu_0}{\lambda_0 + 2\mu_0})\frac{\nabla\varphi_N + i\nabla\psi_N}{h} \cdot \ell$$

and

$$e^{(\varphi_N - t^{-1} + i\psi_N)/h}\mu_0^{-1}\frac{1}{h^2}\nabla(\varphi + i\psi) \otimes \nabla(\varphi + i\psi)d$$

(see [12]).

Assume that the first assumption of (3.5) holds. Then the leading terms of two integrals in (3.7) come from $S(\nabla u_{N,t,h})$ and are determined by

$$\frac{1}{h^4}e^{2(\varphi_N - t^{-1})/h}((\nabla\varphi_N)^2 + (\nabla\psi_N)^2)^2|d|^2. \quad (3.8)$$

On the other hand, if the second assumption of (3.5) holds, then the leading terms in those integrals in (3.7) come from $\nabla \cdot u_{N,t,h}$ and are governed by

$$\frac{2}{h^2}e^{2(\varphi_N - t^{-1})/h}(\nabla\varphi_N)^2|\ell|^2. \quad (3.9)$$

Now the statement (i) and (ii) follow directly from (3.7) and (3.8) or (3.9). The other two cases of (3.5) are treated similarly. $\square$

In view of Theorem 3.1, we are able to reconstruct some part of ∂D by looking into the asymptotic behavior of $E(N,t,h)$ for various t's.

More precisely, let

$$t_{D,N} := \sup\{t \in (0,\infty) : \lim_{h \to 0} E(N,h,t) = 0\}$$

then if $t_{D,N} = \infty$ we have $\Gamma_N \cap D = \emptyset$. On the other hand, if $t_{D,N} < \infty$ then there exists a $p_{D,N} \in \mathcal{D}_{t_{D,N}} \cap \partial D$.

By taking N arbitrarily large (the opening angle of Γ_N becomes arbitrarily small), we can reconstruct even more information of ∂D. A point p on ∂D is said to be *detectable* if there exists a semi-straight line L starting from p such that L does not intersect ∂D except p. For example, if D is star-shaped, every point of ∂D is detectable.

Corollary 3.2. *Every detectable point of ∂D can be reconstructed from Λ_D.*

We refer to [13] for a proof of this corollary. To end this section, we give an algorithm of our reconstruction method.

Step 1. Pick a point $x_0 \notin \bar{\Omega}$ (but close to $\bar{\Omega}$). Given $N \in \mathbb{N}$ and choose the cone Γ_N which intersects Ω.

Step 2. Start with $t > 0$ such that $\mathcal{D}_t \cap \Omega \neq \emptyset$. Construct $u_{N,t,h}$ and determine the Dirichlet data $f_{N,t,h} = u_{N,t,h}|_{\partial\Omega}$.

Step 3. Compute $E(N,t,h) = \int_{\text{supp }(f_{N,t,h})}(\Lambda_D - \Lambda_0)f_{N,t,h} \cdot \bar{f}_{N,t,h}ds$.

Step 4. If $E(N,t,h)$ is arbitrarily small, then increase t and repeat Step 2 and 3; if $E(N,t,h)$ is arbitrarily large, then decrease t and repeat Step 2 and 3.

Step 5. Repeat Step 4 to get a good approximation of ∂D in Γ_N.

Step 6. Move the cone Γ_N around x_0 by taking a different c_N in $\varphi_N = \text{Re}(c_N x^N)$. Repeat Step 2–5.

Step 7. Choose a larger N and a new cone Γ_N. Repeat Step 2–6.

Step 8. Pick a different x_0 and repeat Step 1–7.

4. NUMERICAL RESULTS

4.1. **Preliminaries.** In this section, we provide some computational results based on our method. We shall demonstrate numerical results for two cases – Ω is a rectangle and Ω is an infinite strip. In both cases, we assume that the background parameters λ_0, μ_0 satisfy $\lambda_0(x) \equiv \lambda > 0$ and $\mu_0(x) \equiv \mu > 0$ for all $x \in \Omega$. For such λ_0 and μ_0, we can construct special solutions $u_{N,h}$ satisfying $\mathcal{L}_0 u_{N,h} = 0$ quite explicitly. In other words, we do not need to go through the general procedures given in Section 2. More precisely, for λ_0, μ_0 given here, the corresponding matrices A and Q in (2.1) are reduced to

$$A(x) = \begin{pmatrix} 0 & 0 \\ 0 & \zeta \end{pmatrix}$$

and
$$Q(x) \equiv 0,$$
where $\zeta = \frac{\lambda+\mu}{\lambda+2\mu}\mu^{1/2} > 0$. Therefore, (2.1) can be written as

$$\begin{cases} \Delta w = 0, \\ \Delta g + \zeta \nabla \cdot w = 0. \end{cases} \tag{4.1}$$

To construct special solutions for (4.1), we first choose
$$w = e^{(\varphi+i\psi)/h}w_0,$$
where $w_0 = \nabla\varphi + i\nabla\psi$. To simplify the notations, we denote $\varphi = \varphi_N$ and $\psi = \psi_N$. To check that w satisfies the first equation of (4.1), we note that

$$\Delta\varphi + i\Delta\psi = 0 \quad \text{and} \quad (\nabla\varphi + i\nabla\psi)^2 = 0. \tag{4.2}$$

Therefore, from (4.2) we obtain

$$\begin{aligned} \Delta w &= \Delta(e^{(\varphi+i\psi)/h}w_0) \\ &= \Delta e^{(\varphi+i\psi)/h}w_0 + 2\nabla(e^{(\varphi+i\psi)/h}) \cdot \nabla w_0 + e^{(\varphi+i\psi)/h}\Delta w_0 \\ &= \frac{2}{h}\, e^{(\varphi+i\psi)/h}(\nabla\varphi + i\nabla\psi) \cdot \nabla w_0 + e^{(\varphi+i\psi)/h}\nabla(\Delta\varphi + i\Delta\psi) \\ &= \frac{1}{h}\, e^{(\varphi+i\psi)/h}\nabla(\nabla\varphi + i\nabla\psi)^2 \\ &= 0. \end{aligned}$$

Furthermore, due to (4.2), we observe that

$$\nabla \cdot w = 0.$$

Thus, we simply choose $g \equiv 0$ and the second equation of (4.1) holds. In other words,

$$u_{N,h} = e^{(\varphi_N+i\psi_N)/h}(\nabla\varphi_N + i\nabla\psi_N)$$

satisfies $\mathcal{L}_0 u_{N,h} = 0$. Thus, our simulated (exact) Dirichlet condition is given by

$$f_{N,t,h} = \phi_{N,t}e^{-t^{-1}/h}e^{(\varphi_N+i\psi_N)/h}(\nabla\varphi_N + i\nabla\psi_N)|_{\partial\Omega}.$$

To indicate the dependence of φ_N and ψ_N on the vertex point of the associated cone, in what follows, we will write $\varphi_N = \varphi_N(x, x_0)$ and $\psi_N = \psi_N(x, x_0)$, where x_0 stands for the vertex point.

We now describe our reconstruction strategies. The same procedures were also used in [2] and [13]. In our program, in order to show the numerical results more efficiently without using excessive computational time, we fix $N = 4$ and probe the region Ω by moving the vertex point of the probing cone with $\theta_4 = 0$ (i.e., without rotating the probing

cone). Hence, we first design M different probing cones based on M different vertex points. Remind that each cone is congruent to the cone with vertex at the origin and opening angle $\pi/4$. We then take appropriate h_1 and h_2 with $h_1 > h_2$ and choose a suitable number of probing fronts determined by t_j for $j = 1, \cdots, J$ with $t_j < t_{j+1}$. In each probing cone Γ_m $(m = 1, \cdots, M)$ given above, we construct the Dirichlet data f supported in the intersection of Γ_m and the bottom boundary of $\partial\Omega$ for every h_k and t_j, $k = 1, 2$, $j = 1, \cdots, J$. We now evaluate $E_{j,k} := E(N, t_j, h_k)$ and determine t_n such that

$$E_{n+1,2} > E_{n+1,1}. \tag{4.3}$$

Then the region R_m defined by

$$R_m = \{x \in \Gamma_m : \varphi_N(x, x_0) \le t_n^{-1}\}$$

is the estimated largest region in Γ_m which does not contain the inclusion. So the region $R := \cup_{m=1}^M R_m$ is the estimated largest region with absence of inclusion with a given sweeping scheme. We would like to point out that condition (4.3) is our rule of thumb in determining whether the level curve $\varphi_N(x, x_0) = t^{-1}$ intersects the inclusion in our numerical experiments. It is not equivalent to Theorem 3.1, but based on the reasoning that $E(N, t, h)$ is *exponentially decaying* when $\varphi_N(x, x_0) = t^{-1}$ stays away from the inclusion and *exponentially growing* when $\varphi_N(x, x_0) = t^{-1}$ intersects the inclusion.

To show the effect of noise to our method, we add appropriate noise to the simulated data. We consider the form of noise given in [2]. To be precise, let $\eta : [-1, 1] \mapsto \mathbb{C}$ be a random function defined by

$$\eta(s) = \sum_{k=-32}^{32} (a_k + ib_k)e^{iks\pi/2},$$

where $a_k, b_k \sim \mathcal{N}(0, 1)$ are normally distributed random numbers. The number 32 in η is chosen to roughly model a collection of 32 electrodes on the bottom boundary of Ω. Measurement noise is modeled by $\Lambda_D f$ by $\Lambda_D f + c\eta$ with

$$c = \frac{A\|\Lambda_D f\|_\infty}{\|\eta\|_\infty},$$

where $A > 0$. Finally, we would like to point out that in our simulation, a big chunk of computational time is used to obtain the simulated data. This is the forward problem. Once having the simulated data, the inverse procedure is rather trivial. In order to obtain desired accuracy on the simulated data and be able to adapt to different shapes of inclusions, we use the finite element method (FEM) to solve the forward problem. In our FEM program, we perform the grid refinement near

the boundary and the inclusion to ensure the accuracy of the simulated data (see Figure 4.1 for example).
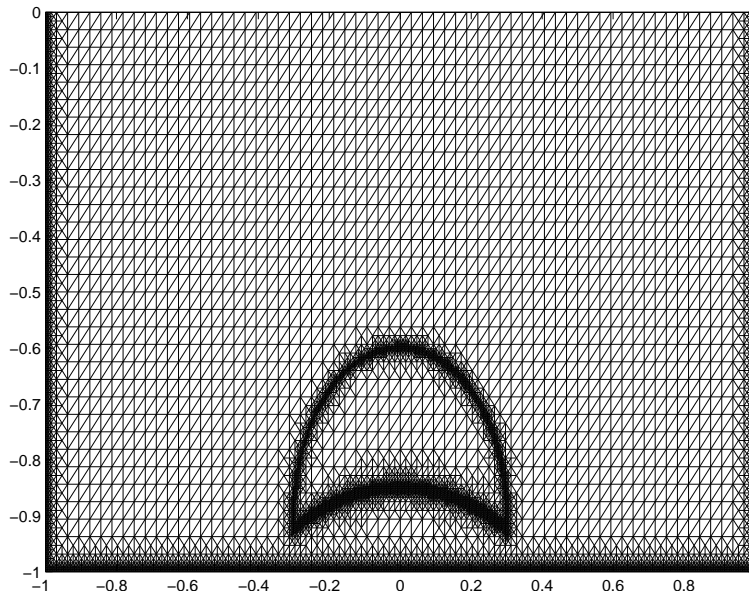

FIGURE 4.1. Example of our FEM meshes.

4.2. Ω **is a rectangle.** In our numerical computations, we take the domain

$$\Omega = \{(x_1, x_2) : -1 < x_1 < 1, -1.01 < x_2 < -0.01\}.$$

We shall use the Dirichlet data localized on $\{(x_1, -0.01) : -1 < x < 1\}$ (top boundary) $\{(x_1, -1.01) : -1 < x < 1\}$ (bottom boundary). To this end, we choose vertex points from $\{x_2 = -1.02\}$ and $\{x_2 = 0\}$, respectively. Let $x_0 = (x_{0,1}, x_{0,2})$ denote the vertex point and we write

$$\rho_4(x, x_0) := \varphi_4(x, x_0) + i\psi_4(x, x_0) = ((x_1 - x_{0,1}) + i(x_2 - x_{0,2}))^4.$$

Thus, the probing fronts are level curves of φ_4. In Figure 4.2, we show some probing fronts with nonzero Dirichlet condition on the bottom. To set up the Dirichlet condition, we ignore the cut-off function $\phi_{N,t}$ and take

$$f_{N,t,h}|_{\partial\Omega} = \begin{cases} e^{(\rho_4(x,x_0)-t^{-1})/h}\nabla\rho_4(x, x_0), & \text{for } (x_1, x_2) \in \partial\Omega_{\text{obs}}, \\ 0, & \partial\Omega \setminus \partial\Omega_{\text{obs}}, \end{cases}$$

where $\partial\Omega_{\text{obs}}$ is determined by x_0. For example, if $x_0 = (0, 0)$, then

$$\partial\Omega_{\text{obs}} = \{(x_1, x_2) : -1.01 \times \tan(\frac{\pi}{8}) < x_1 < 1.01 \times \tan(\frac{\pi}{8}),\ x_2 = -1.01\}.$$
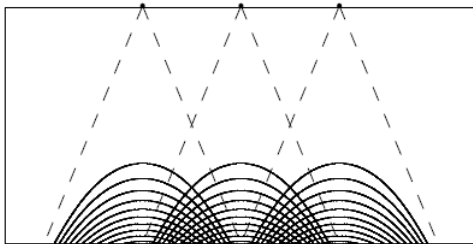
FIGURE 4.2. Probing fronts of our numerical method.
In this figure, the nonzero Dirichlet condition is on the
bottom boundary.

In the following figures, we show our reconstruction method for three
cases with different inclusions. As we mentioned above, due to compu-
tational costs, we only provide numerical results obtained by putting
nonzero Dirichlet condition on either the top or the bottom bound-
aries. In conventional expression, we describe the elastic medium by
the Young's modulus E and the Poisson ratio ν. The relation between
(E, ν) and (λ, μ) is given by

$$\lambda = \frac{E\nu}{1 - \nu^2} \quad \text{and} \quad \mu = \frac{E}{2(1 + \nu)}.$$

In our simulations, we take $(E, \nu) = (6 \times 10^6, 0.45)$ for the background
medium (gray area) and $(E, \nu) = (6 \times 10^7, 0.45)$ inside of the inclusions
(black area).

We now want to make some remarks on the figures showing above.
Since we are only probing the region from the top and the bottom
boundaries, we are unable to resolve the inclusion-free near the left
and the right boundaries. Thus, the area on near those boundaries are
black. Moving the nonzero Dirichlet condition $f_{N,t,h}$ to those places will
certainly improve the resolution of the inclusion. But we need to pay
the price of at least double the computational cost. We believe that
showing the figures obtained by probing from the top and the bottom
is sufficient to demonstrate the essential ideas of our method.

4.3. Ω **is a strip.** Here we assume $\Omega = \{(x_1, x_2) : -\infty < x_1 < \infty, \ -1.01 < x_2 < -0.01\}$. In order to get the simulated data in
this case, we need to impose appropriate artificial boundary conditions
in the x_1 direction. We now rewrite elasticity system (1.2) or (1.3) into

$$\begin{pmatrix} \lambda + 2\mu & 0 \\ 0 & \mu \end{pmatrix} \partial_1^2 u + \begin{pmatrix} 0 & \lambda + \mu \\ \lambda + \mu & 0 \end{pmatrix} \partial_1 \partial_2 u + \begin{pmatrix} \mu & 0 \\ 0 & \lambda + 2\mu \end{pmatrix} \partial_2^2 u = 0.$$
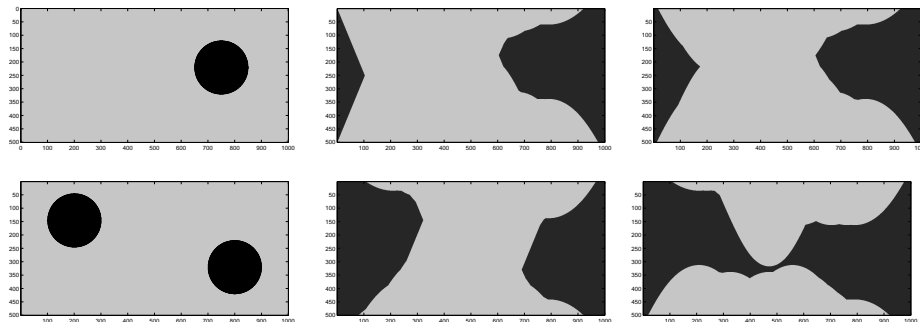
$$(4.4)$$

FIGURE 4.3. The first column represents the actual location of the inclusion. The second column is the numerical reconstruction with noiseless simulated data. The third column is the numerical reconstruction with noisy data with $A = 0.01\%$. All gray areas are inclusion-free regions.

The characteristic polynomial related to (4.4) is

$$P(\xi) := \begin{pmatrix} \lambda + 2\mu & 0 \\ 0 & \mu \end{pmatrix} \xi_1^2 + \begin{pmatrix} 0 & \lambda + \mu \\ \lambda + \mu & 0 \end{pmatrix} \xi_1 \xi_2 + \begin{pmatrix} \mu & 0 \\ 0 & \lambda + 2\mu \end{pmatrix} \xi_2^2,$$

which is a symmetric quadratic matrix polynomial. Motivated by the factorizations of symmetric quadratic matrix polynomials, by some computations, we can see that

$$P(\xi) = (I\xi_1 - B^T\xi_2) \begin{pmatrix} \lambda + 2\mu & 0 \\ 0 & \mu \end{pmatrix} (I\xi_1 - B\xi_2)$$

with

$$B = \begin{pmatrix} 0 & -1 \\ 1 & 0 \end{pmatrix}.$$

Therefore, system (4.4) can be factored into

$$(I\partial_1 - B^T\partial_2) \begin{pmatrix} \lambda + 2\mu & 0 \\ 0 & \mu \end{pmatrix} (I\partial_1 - B\partial_2)u = 0. \qquad (4.5)$$

In view of (4.5), on any artificial boundary $x_1 = a$, we impose condition

$$\partial_1 u(a, x_2) - B\partial_2 u(a, x_2) = 0. \qquad (4.6)$$

Explicitly, in our numerical simulation, we truncate the infinite strip Ω into a rectangle considered in section 4.2. For example, in case of

$x_0 = (0, 0)$, we impose the boundary condition as follows:

$$\begin{cases} u = e^{(\rho_4(x,x_0)-t^{-1})/h}\nabla\rho_4(x, x_0) & (x_1, x_2) \text{ in } \partial\Omega_{\text{obs}}, \\ \partial_1 u(1, x_2) = B\partial_2 u(1, x_2) & \text{for } -0.01 < x_2 < -1.01, \\ \partial_1 u(-1, x_2) = B\partial_2 u(-1, x_2) & \text{for } -0.01 < x_2 < -1.01, \\ u = 0 & \text{elsewhere.} \end{cases} \quad (4.7)$$

We will indicate how to implement boundary condition (4.7) in the FEM method in the appendix. The computational results for the strip case with noiseless and noisy data are given in Figure 4.4.
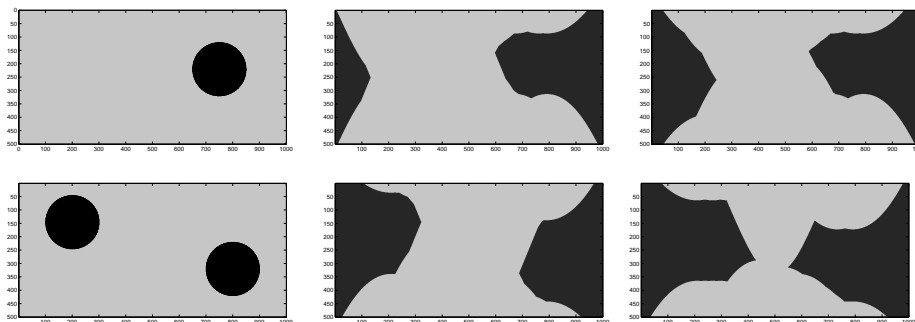

FIGURE 4.4. The first column represents the actual location of inclusions. The second column is the numerical reconstruction with noiseless simulated data. The third column is the numerical reconstruction with noisy data with $A = 0.01\%$. All gray areas are inclusion-free regions.

4.4. **Ill-posedness.** Supported by numerical evidence, it is widely believed that when the unknown object is far away from the boundary, the determination problem by boundary measurements is more ill-posed than the case where the object is near the boundary. The following figures give further examples of this interesting phenomenon. In Figure 4.5, we can see that the lower part of the inclusion is clearly resolved; while, the upper part of the inclusion is difficult to detect.

5. CONCLUSIONS

In this article, we present a numerically feasible reconstruction algorithm for the determination of inclusions by boundary measurements for the two-dimensional isotropic elasticity system. The domain can also be unbounded. We point out that the same method works for the cavity case. Our method depends on a new type of CGO solutions for
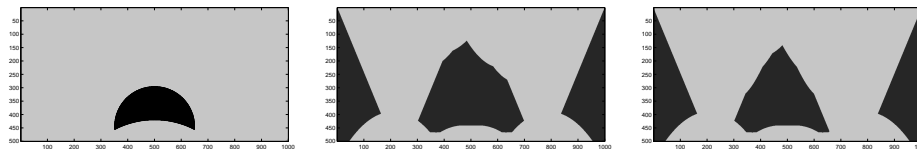
FIGURE 4.5. The first column is the actual location of the inclusion. The second column is the numerical reconstruction with noiseless simulated data when Ω is a rectangle. The third column is the numerical reconstruction with noiseless simulated data when Ω is a strip. All gray areas are inclusion-free regions.

the elasticity system. Numerical results show the actually implementation of the method with noiseless or noisy data simulated data derived from the FEM.

To be able to effectively demonstrate our method without excessively computational efforts, we choose $N = 4$ and probe the region from the top and the bottom boundaries in the numerical simulation. It is of course very natural to choose large N and also probe the region from all sides. However, obtaining the simulated data for this improvement will be a very time-consuming task.

From the numerical results, our method is very effective in determining parts of the object near the boundary even when the domain is unbounded. Its flexibility gives us another technique that can potentially be used in real applications such as medical imaging and nondestructive evaluation.

APPENDIX A

In this appendix, we show how to implement the artificial boundary condition (4.6) in the FEM. Denote $u = (u_1, u_2)^T$. Let Γ_D be the boundary with imposed Dirichlet data $f_{N,t,h}$ and Γ_A denote the artificial boundary. From the variational formulation of the equation (1.2), the isotropic elastic system on the truncated domain in section 4.3 can be

written as follows:

$$
\int_\Omega \begin{pmatrix} \partial_1 v_1 \\ \partial_2 v_2 \\ \partial_2 v_1 + \partial_1 v_2 \end{pmatrix}^T \begin{pmatrix} \lambda + 2\mu & \lambda & 0 \\ \lambda & \lambda + 2\mu & 0 \\ 0 & 0 & \mu \end{pmatrix} \begin{pmatrix} \partial_1 u_1 \\ \partial_2 u_2 \\ \partial_2 u_1 + \partial_1 u_2 \end{pmatrix} dx
$$
$$
- \int_{\partial\Omega} v_1 \left(\lambda \nabla \cdot u + 2\mu \partial_1 u_1, \mu \left(\partial_2 u_1 + \partial_1 u_2 \right) \right) \cdot \mathbf{n} \ ds
$$
$$
- \int_{\partial\Omega} v_2 \left(\mu \left(\partial_2 u_1 + \partial_1 u_2 \right), \lambda \nabla \cdot u + 2\mu \partial_2 u_2 \right) \cdot \mathbf{n} \ ds = 0
$$

$$\text{(A.1)}$$

where v_1, v_2 are test functions in $H^1_{0,\Gamma_D}(\Omega) = \{ v \in H^1(\Omega) |\ v(x) = 0 \text{ for } x \in \Gamma_D \}$. From (4.6), one has that

$$
\partial_1 u_1 + \partial_2 u_2 = \nabla \cdot u = 0 \quad \text{and} \quad \partial_1 u_2 - \partial_2 u_1 = 0, \qquad \text{(A.2)}
$$

on Γ_A. Since the artificial boundary consists of line segments along the x_2-direction only, by (A.2), the partial derivatives $\partial_1 u_1$ and $\partial_1 u_2$ are replaced by $-\partial_2 u_2$ and $\partial_2 u_1$, respectively. Thus the variational formulation (A.1) becomes

$$
\int_\Omega \begin{pmatrix} \partial_1 v_1 \\ \partial_2 v_2 \\ \partial_2 v_1 + \partial_1 v_2 \end{pmatrix}^T \begin{pmatrix} \lambda + 2\mu & \lambda & 0 \\ \lambda & \lambda + 2\mu & 0 \\ 0 & 0 & \mu \end{pmatrix} \begin{pmatrix} \partial_1 u_1 \\ \partial_2 u_2 \\ \partial_2 u_1 + \partial_1 u_2 \end{pmatrix} dx
$$
$$
+ \int_{\Gamma_A} 2\mu v_1 \left(\partial_2 u_2, -\partial_2 u_1 \right) \cdot \mathbf{n} \ dx_2 - \int_{\Gamma_A} 2\mu v_2 \left(\partial_2 u_1, \partial_2 u_2 \right) \cdot \mathbf{n} \ dx_2 = 0.
$$

$$\text{(A.3)}$$

As a result, the standard finite element discretization procedure can now be employed in (A.3).

References

[1] A.P. Calderón, *On an inverse boundary value problem*, in *Seminar on Numerical Analysis and its Applications to Continuum Physics*, Río de Janeiro, 1980.

[2] T. Ide, H. Isozaki, S. Nakata, S. Siltanen, and G. Uhlmann, *Probing for electrical inclusions with complex spherical waves*, Comm. Pure Appl. Math, textbf60 (2007), 1415-1442.

[3] M. Ikehata, *Reconstruction of inclusion from boundary measurements*, J. Inv. Ill-posed Problems, **10** (2002), 37-65.

[4] M. Ikehata, *A remark on an inverse boundary value problem arising in elasticity*, preprint.

[5] M. Ikehata, *Inverse conductivity problem in the infinite slab*, Inverse Problems, **17** (2001), 437-454.

[6] M. Ikehata, *Mittag-Leffler's function and extracting from Cauchy data*, Inverse problems and spectral theory, 41-52, Contemp. Math., **348**, Amer. Math. Soc., Providence, RI, 2004.

[7] M. Ikehata and S. Siltanen, *Electrical impedance tomography and Mittag-Leffler's function*, Inverse Problems, **20** (2004), 1325-1348.

[8] G. Nakamura and G. Uhlmann, *Global uniqueness for an inverse boundary problem arising in elasticity*, Invent. Math., **118** (1994), 457-474.

[9] M. Salo and J.-N. Wang, *Complex spherical waves and inverse problems in unbounded domains*, Inverse Problems, **22** (2006), 2299-2309.

[10] G. Uhlmann, *Developments in inverse problems since Calderón's foundational paper*, Harmonic Analysis and Partial Differential Equations (*Essays in Honor of Alberto P. Calderón*), 295-345, The University of Chicago Press, Chicago, 1999.

[11] G. Uhlmann, *Commentary on Alberto P. Calderó's paper: On an Inverse Boundary Value Problem* to appear, Selecta, published by AMS, edited by A. Bellow, C.E. Kenig and P. Malliavin.

[12] G. Uhlmann and J.-N. Wang, *Complex spherical waves for the elasticity system and probing of inclusions*, SIAM J. Math. Anal., **38** (2007), 1967–1980 .

[13] G. Uhlmann and J.-N. Wang, *Complex geometrical optics solutions and reconstruction of discontinuities*, to appear SIAM J. Appl. Math.

DEPARTMENT OF MATHEMATICS, UNIVERSITY OF WASHINGTON, BOX 354305, SEATTLE, WA 98195-4350, USA.

E-mail address: gunther@math.washington.edu

DEPARTMENT OF MATHEMATICS, TAIDA INSTITUTE FOR MATHEMATICAL SCIENCES, AND NCTS (TAIPEI), NATIONAL TAIWAN UNIVERSITY, TAIPEI 106, TAIWAN.

E-mail address: jnwang@math.ntu.edu.tw

DEPARTMENT OF APPLIED MATHEMATICS, NATIONAL CHIAO TUNG UNIVERSITY, HSINCHU 300, TAIWAN.

E-mail address: ctw@math.nctu.edu.tw